Japanese Journal of Applied Physics
Vol. 43, No. 10, 2004, pp. 7261–7266

Requirements of Neutral Beam Source Regarding Gas Pressure and Neutral Angle for Nanoscale Etching

Sung Jin KIM, Hae June LEE[1], Geun Young YEOM[2] and Jae Koo LEE*

Department of Electronic and Electrical Engineering, Pohang University of Science and Technology, Pohang 790-784, South Korea
[1]*School of Electrical and Computer Engineering, Pusan National University, Busan 609-735, South Korea*
[2]*Department of Materials Engineering, Sungkyunkwan University, Suwon 440-746, South Korea*

(Received April 7, 2004; revised June 3, 2003; accepted June 16, 2004; published October 8, 2004)

Neutral beam etching is proposed as a candidate process for reducing plasma-process-induced damage (PPID) in nanoscale devices. The requirements of neutral beam properties for high-performance etching are investigated using a two-dimensional particle code. The neutral beam is generated using a plasma-source ion gun and low-angle reflectors. Neutral fluxes from both the neutral beam source and background gases are calculated as functions of gas pressure. The optimal pressure regime which is related to the rate of sidewall etching is suggested. In three-dimensional charge-up simulations, it is observed that the etching rate decreases with decreasing trench size due to the surface charging effect. However, a smaller reduction in the etching rate is observed experimentally in neutral beam etching. The influence of the neutral angle distribution on the etching rate is investigated using a Poisson random variable model. A low directional ratio of the neutral angle results in a low etching rate and a large decrease in etching rate as trench width decreases. Therefore, a pressure of less than 0.5 mTorr and a directional ratio of neutral angle higher than 50% are required for high-performance neutral beam etching.
[DOI: 10.1143/JJAP.43.7261]

KEYWORDS: neutral beam, simulation, charge-up damage, etching, pressure, angle distribution

1. Introduction

Plasma etching is widely used in the manufacture of ultralarge-scale integrated circuits. Various plasma sources, such as capacitively coupled plasmas (CCP), inductively coupled plasmas (ICP), electron cyclotron resonance (ECR) plasmas, and helicon plasmas, have been studied in the past. Plasma etching requires a high etching rate, anisotropy, good selectivity, uniformity across the wafer, and process reproducibility.[1,2] However, plasma etching processes that use charged particles, in particular, reactive ion etching (RIE), inevitably produce plasma-process-induced damage (PPID).[3,4] As device size shrinks toward the nanoscale, the effect of PPID on the device characteristics becomes more serious. PPID, such as notching, earlier etching stop, and RIE lag, is contributed to by the difference in the motions of ions and electrons in the narrow trench.[5–7] The etching rate and etching profile depend on feature size and aspect ratio. Typically, RIE lag represents the dependence of the etching rate on the shape of the trench being etched. Narrower trenches are etched more slowly than wider trenches. RIE lag is produced by ions and radical depletion.[3]

Neutral beam etching is proposed as a candidate process for solving the problems related to the use of charged particles in etching. Various neutral beams, such as a hyperthermal atomic beam,[8,9] a neutral beam produced by ion-neutral scattering,[10,11] and a neutral beam produced by ion-electron recombination,[12] have been studied. In neutral beam etching, the energy and incidence angle of radicals are directly controlled.

In this study, the requirements of neutral beam properties which are related to the pressure and the incidence angle of the neutral beam are investigated for anisotropic etching by simulation. We have performed a neutral beam simulation[13] using a modified Xgrafic object oriented particle-in-cell (XOOPIC) code.[14] The neutral beam source was generated using a plasma source ion gun and low-angle reflectors.[15] Ions accelerated using the ion gun were neutralized by collision with the reflectors. Reflection characteristics were calculated using the transport of ions in matter (TRIM) code.[16] Etching properties were estimated from the characteristics of the neutral beam in the neutral beam simulation.

We describe a method of neutral beam simulation in §2. The effect of gas pressure on sidewall etching is described in §3. RIE lag due to the influence of surface charging on reactive ion etching, as predicted by a three-dimensional charge-up simulation, is described in §4. The change in etching rate with respect to the neutral beam angle is also discussed in §4. The requirements of the neutral beam source for nanoscale etching are suggested in §5.

2. Simulation of Neutral Beam Source

A plasma source with an ion gun and low-angle reflectors is used as the neutral beam source. A schematic of the low-angle-reflector (LAR) neutral-beam source is shown in Fig. 1. The ion gun is composed of two grids controlled by an external voltage source. To extract positive ions, a positive voltage is applied to the first grid and a negative or zero voltage is applied to the second grid. Only positive ions are extracted through the holes by the electric field between the two grids. As the ions approach the high-work function

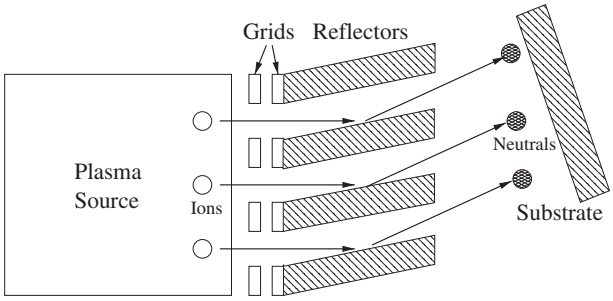

Fig. 1. Schematic configuration of neutral beam source.

*E-mail address: jkl@postech.ac.kr

metal, they are neutralized through a resonant neutralization process and an Auger capture process.

The neutral beam generation simulation is comprised of an ion gun simulation and a neutral beam simulation. The ion gun simulation is conducted separately from the neutral beam simulation because of the different mesh sizes used in the simulations. The ion energy and the angle distributions are calculated using the XOOPIC code, which yields satisfactory estimations of the energy and angle distributions of ions and electrons. These are the input parameters for the neutral beam simulation. Since the phenomenon of collisions between ions and reflectors is very complicated and there is a lack of theoretical and experimental data for ions with energies ranging from 10 to 1000 eV, it is difficult to determine the rates of reflection and neutralization. Therefore, we have considered the use of a computational model using the Monte Carlo method of random sampling known as TRIM.[16,17] Reflection characteristics, such as the reflection coefficient, and the energy and angle of the reflected particle, calculated using the TRIM code, are appended to the XOOPIC code. The reflection coefficient depends on the incident energy and angle of ions. The energy of a reflected particle is approximately 70% of the incident ion energy. The reflected angle distribution has a cosine distribution, as determined from the incident ion angle.[18,19] It is assumed that most of the reflected particles are neutral on the basis of Hagstrum's model and the work of Helmer.[20,21]

In our simulation, the grid width of the ion gun is 1.2 mm, and the interval between the holes is 0.9 mm. The hole size is 4 mm. The angle and length of the reflectors are 5° and 46 mm, respectively. The reflector length is set by considering the hole size and reflector angle to reduce the number of ions which undergo no collision with the reflectors and the number of secondary collisions of neutrals. Ar gas is used for obtaining the fundamental characteristics of the reflected neutral beam.

3. Effect of Gas Pressure on Neutral Beam Etching

The chamber gas pressure has an influence upon directional etching on Si wafers. The neutral flux from the background gases, which is randomly isotropic, induces directional etching. Generally, the neutral flux is linearly proportional to the etching rate in the case of SF_6 gas.[22] For Si etching using a neutral beam source, the neutral flux from the neutral beam source should be larger than that from the background gases. We performed the neutral beam simulation to investigate the relation between the generated neutral beam and the background gases as a function of gas pressure.

Figure 2 shows neutral flux as a function of gas pressure. A low gas pressure creates a low neutral flux in the LAR neutral source, due to the decrease in the ion flux from the plasma source. The neutral flux from the background gases (line marked by circles) also decreases with decreasing gas pressure. It is calculated as follows:

$$J_F = \frac{N_F}{4}\left(\frac{8kT_g}{\pi M}\right)^{\frac{1}{2}}, \quad (1)$$

where J_F and N_F are the neutral flux and the neutral density, respectively. The rate of decrease of the neutral flux from the background gases is higher than that from the neutral beam source, as shown in Fig. 2. At 1 mTorr, the neutral fluxes from the background gases and the LAR neutral beam source are nearly the same. The neutral flux from the background gases leads to isotropic etching. Undercutting or bowing occurs when the high-pressure neutral beam source is used. Therefore, the anisotropic etching profile is obtained at a pressure less than 0.5 mTorr. In SF_6 gas, the chemical etching rate of Si[22] is defined by Ninomiya *et al.*[23]

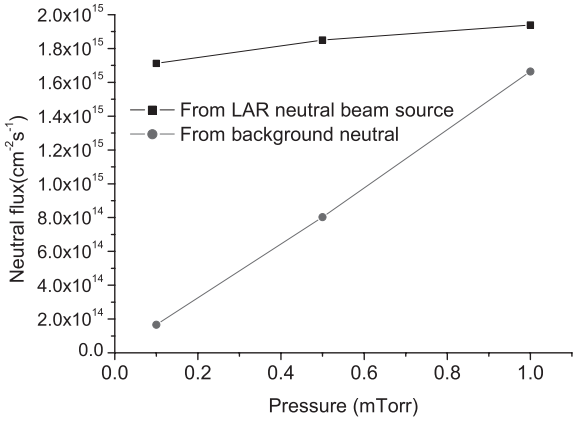

Fig. 2. Neutral flux versus pressure. The line marked by rectangles is the neutral flux from a low-angle-reflector neutral beam source. The dashed line marked by circles is the neutral flux from the background neutral gases.

$$\log(R_{Si}) = -11.35 + \log(N_F), \quad (2)$$

where R_{Si} is the etching rate (nm/min) of Si described as a function of neutral density. It can be represented as a function of neutral flux by using the correlation between neutral flux and neutral density. The chemical etching rate as a function of neutral flux,[22] as derived from eqs. (1) and (2), is

$$R_{Si} = (5.20 \times 10^{12.35})^{-1} J_F. \quad (3)$$

It is linearly proportional to the neutral flux. In our experiment, the Si etching rate at 0.3 mTorr is 110 nm/min.[24] As calculated using eq. (3), the neutral flux is $1.28 \times 10^{15}\ cm^{-2}s^{-1}$. This is similar to our simulation result (see Fig. 2). Considering a gas pressure less than 0.5 mTorr in neutral beam etching, the neutral flux from the neutral beam source is larger than that from the background gases. Although low pressure leads to a low etching rate, low pressure is required to improve the performance of neutral beam etching in regard to the anisotropic etching profile.

4. Etching Rate Variation Due to Charge-Up Effect and Neutral Beam Angle

4.1 Analysis of RIE lag from three-dimensional charge-up simulation

Narrow trenches are etched more slowly than wide trenches by RIE. It is well known that some mechanisms of RIE lag are Knudsen transport of neutrals, ion shadowing, neutral shadowing, differential charging of insulating microstructures and surface diffusion.[3] As the size of features shrinks toward the nanoscale, the role of each mechanism of RIE lag should be considered to obtain a good etching profile. We have determined, using a three-dimensional

charge-up simulation,[25] that charge-up in a narrow trench affects the etching rate. In the charge-up simulator, the Laplace equation for electric field calculations is used, because the space charge is sufficiently small to be neglected in the trench. The time scale of etching is longer than that of charge-up, and thus etching is negligible during the charge-up potential transient time. The surface current is also neglected. There are six boundary planes: the left ($x = 0$), the right ($x = x_{max}$), the back ($z = z_{max}$), the front ($z = 0$), the top ($y = y_{max}$), and the bottom ($y = 0$) planes. These boundary conditions are used as follows: at the left, the right, the back, and the front boundaries, the Neumann boundary conditions, $\nabla V = 0$, and the periodic boundary conditions, $V_{left} = V_{right}$, $V_{back} = V_{forth}$, are adopted, and at the top and the bottom boundaries, the Dirichlet boundary conditions, $V_{top} = 0$, $V_{bottom} = 0$, are used. The energy and angular distributions of ions and electrons are used for input data in the charge-up code.

For our charge-up simulation, the energy and angular distribution of charged particles are supplied from a CCP source simulation, a one-dimensional cylindrical particle-in-cell (PIC) code. In the RF-CCP source simulation, the frequency and pressure are 27 MHz and 20 mTorr, respectively. The RF voltage and the gap size between the two electrodes are 400 V and 2 cm, respectively. The area ratio of the two electrodes is 1 : 4. The energy and the angular distributions of the electrons and ions are shown in Figs. 3(a) and 3(b). The average energies of electrons and ions are 6.44 eV and 154 eV and the average angles of the electrons and ions are 43.9° and 7.77°, respectively. The energy and the angular distribution of the electrons and ions are applied to the three-dimensional charge-up simulation.

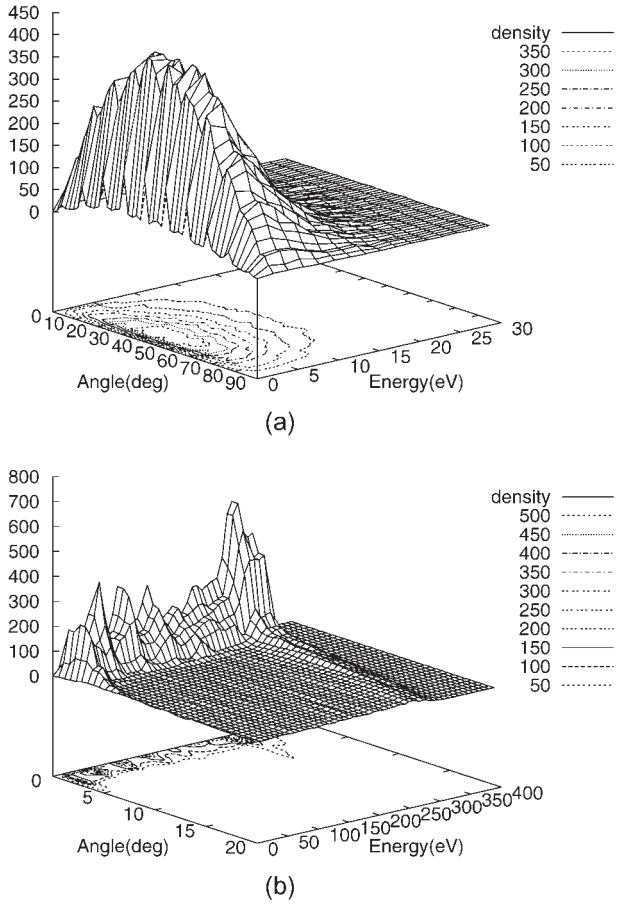

Fig. 3. Energy and angular distributions: (a) electrons and (b) ions. Pressure of 27 MHz RF-CCP is 20 mTorr.

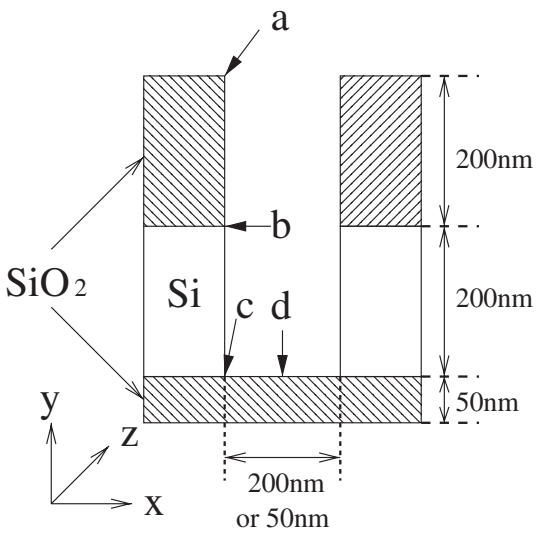

Fig. 4. Positions where potentials are observed in the trench across the center of 200-nm-wide or 50-nm-wide trench in z-direction. The length in z-direction is the same as that in x-direction.

The trench shown in Fig. 4 is formed across the center of a 200 nm or 50 nm trench in the z-direction. The length of the trench in the z-direction is the same as that in the x-direction. It is composed of silicon and SiO_2. The potential at four points in the trench is measured. Potential histories in the 200 nm and 50 nm trench are shown in Figs. 5(a) and 5(b), respectively. The potential at the bottom of trench (solid line marked by d) is larger than at the top of trench (dash-dot line marked by a), as shown in Fig. 5(a). This is due to the difference between ion and electron motion. Electron shading is exhibited at times less than 0.4 ms. In Fig. 5(b), the high potential at the bottom of the trench leads to substantial changes in ion flux. As the trench size decreases, electrons which have isotropic motion are unlikely to reach the bottom. Thus, the potential of the 50 nm trench is larger than that of the 200 nm trench. These different potentials affect the ion flux at the bottom of the trenches. Ion fluxes at the bottom of the 200 nm and 50 nm trenches are shown in Figs. 6(a) and 6(b). The majority of ions are accumulated in the center of the trenches. The potentials at the centers of the bottoms of the trenches are larger than those at the edges of the bottoms. This causes serious sidewall etching such as notching. The etching rate is proportional to the ion flux in reactive ion etching. The etching rate for the 200 nm trench is higher than that for the 50 nm trench because of the high potential formed in the narrower trench. In this case, the effects of neutral radicals are neglected and only surface charge is considered. The experimental result for RIE lag is shown in Fig. 7(a). Poly-Si/SiO_2 is etched by ICP. The RF power and bias voltage are 700 W and −75 V, respectively. Pure SF_6 gas is used at 5 mTorr. The etching rate decreases as the feature size diminishes. This is explained by the potential difference from the surface charge.

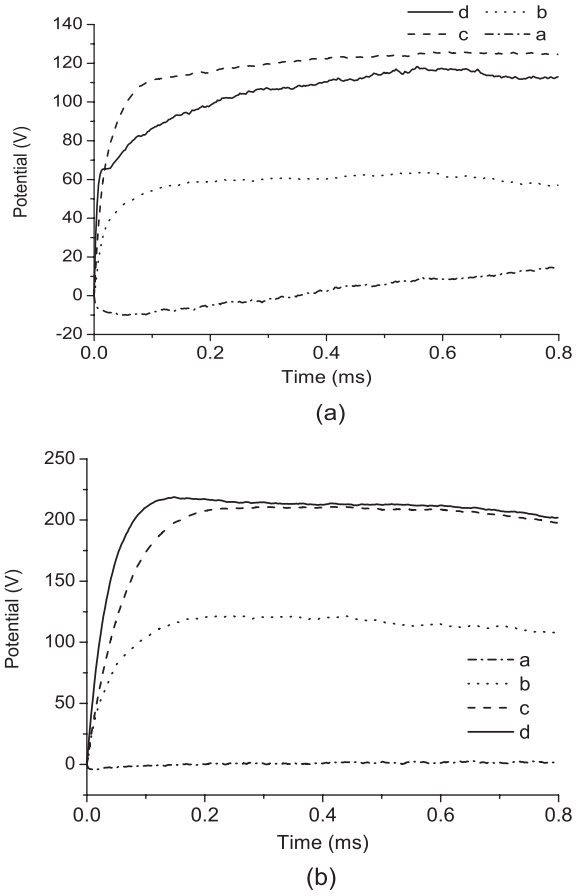

Fig. 5. Potential histories by three-dimensional charge-up simulation: (a) 200 nm and (b) 50 nm trenches.

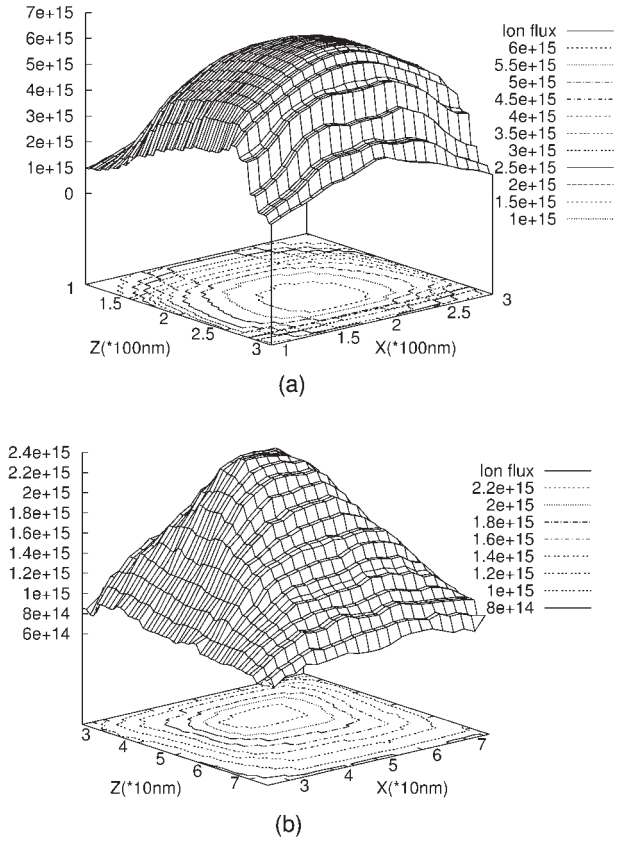

Fig. 6. Ion flux in the bottom of (a) 200 nm and (b) 50 nm trenches.

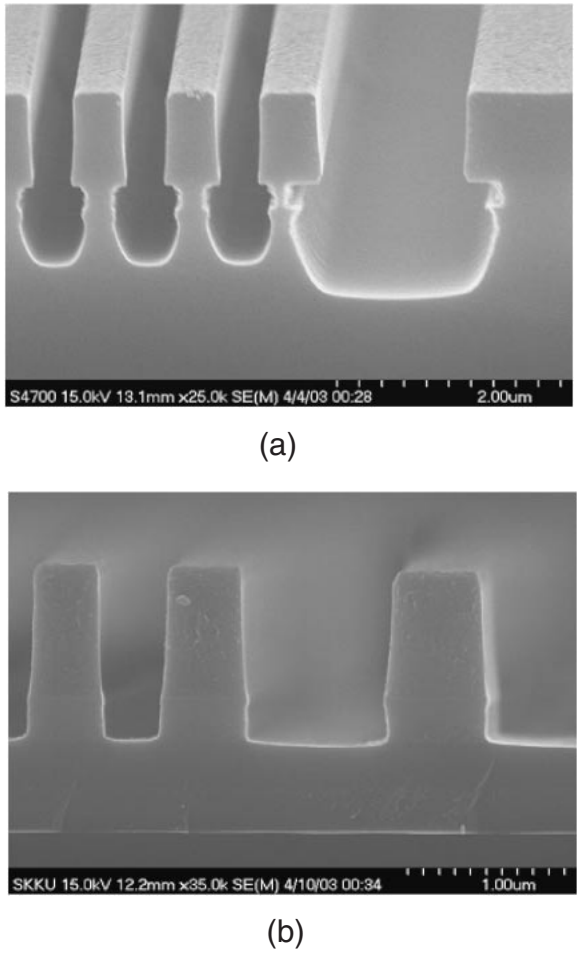

Fig. 7. SEM micrograph of poly-Si/SiO_2 etching profile: (a) ICP etching and (b) neutral beam etching.

4.2 *Effect of neutral angle in neutral beam etching*

Neutral beam etching does not produce PPID, unlike etching using charged particles. The energy and angle of the neutral beam are easily controllable for etching of the nanoscale trench. Poly-Si/SiO_2 etched using a neutral beam is shown in Fig. 7(b). The RF power and reflector angle are 400 W and 5°, respectively. SF_6 gas is used at a pressure of 0.3 mTorr. The grid voltages of the ion gun are 400 V and −100 V. The low gas pressure (0.3 mTorr) results in anisotropic etching. A difference in etching rate is not exhibited at high neutral angles as the feature size changes. It is difficult to measure the neutral angle distribution in the experiment. The directional ratio of the neutral beam angle is more than 50%, as determined from the simulation result. The directional ratio of the neutral beam angle is defined as the number ratio of neutrals having 0° over total neutrals. The neutral angle is an important factor for reducing sidewall etching and the change in etching rate with respect to feature size.

We have observed requirements related to the neutral beam angle for high-performance neutral beam etching. The neutral angle is modeled with the Poisson random variable as

$$p_k = \frac{\alpha^k}{k!} e^{-\alpha}, \quad k = 0, 1, 2, \ldots \tag{4}$$

and

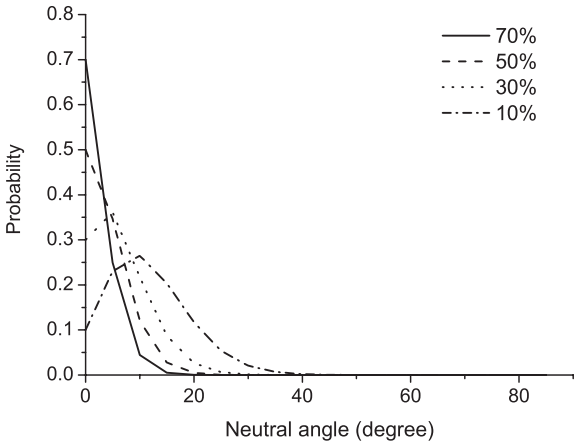

Fig. 8. Neutral angle distributions modeled using Poisson random variable.

$$\alpha = \ln(DR) > 0, \tag{5}$$

where *DR* is the directional ratio of the neutral beam angle and α is determined by the directional ratio of the neutral beam angle. The angle is defined by k multiplied by 5°, which defines the maximum angle. The angular distributions of the neutral beam, which are similar to the neutral angle distribution obtained by our neutral beam simulation, are shown in Fig. 8. The neutral beam angular distribution is affected by variations in the directional ratio. The flux and energy distribution of the neutral beam, which are obtained by the neutral beam simulation described in §2, are used. The neutral flux by variations in neutral angle distribution is calculated for the 200 nm and 50 nm trenches with the trench depth of 400 nm. Reflection data, such as reflection coefficient, energy, and angular distribution, calculated using the TRIM code, are applied to our simulation to consider the sidewall reflection of neutral injected into the trench. Neutral diffusion into the trench is neglected. Neutral flux as functions of trench position and directional ratio is shown in Fig. 9. As the directional ratio of the neutral angle decreases, the neutral flux arriving at the bottom of the trench decreases and the gradient of the neutral flux increases in the trench. The change in the neutral flux in the 50 nm trench [see Fig. 9(b)] is greater than that in the 200 nm trench [see Fig. 9(a)] with the variation of the directional ratio of the neutral angle. This is due to the effect of large-angle neutral shadowing. Although the change in neutral flux as a function of neutral angle is greater in the 50 nm trench, the change in neutral flux as a function of trench position becomes smaller. However, the etching rate also decreases because of the low neutral flux.

In comparisons of the 50 nm and 200 nm trenches, the ion flux ratio in reactive ion etching and the neutral flux ratio in neutral beam etching are shown in Figs. 10(a) and 10(b). The flux ratio is defined as the ratio of the flux in the 200 nm trench to the flux in the 50 nm trench. The ion flux ratio is calculated using the charge-up simulation described in §4.1 and is shown in Fig. 10(a). In reactive ion etching, the gradient of the ion flux ratio becomes large because charged particles increase the potential in the trench. It causes PPID such as RIE lag, and microloading. In neutral beam etching, the high directional ratio of the neutral angle reduces the

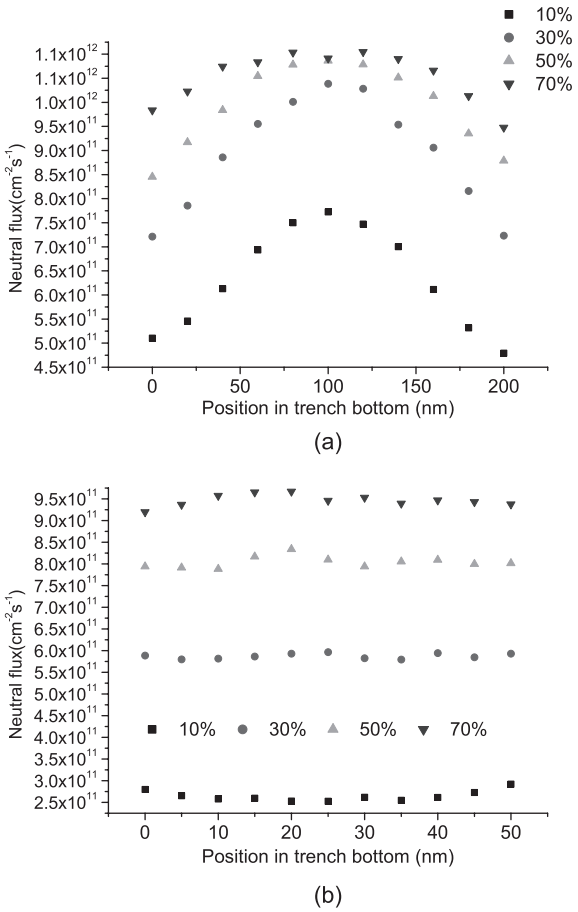

Fig. 9. Neutral flux as a function of directional ratio of neutral angle: (a) 200 nm and (b) 50 nm trenches.

gradient of the neutral flux ratio, as shown in Fig. 10(b). The change in the etching rate of neutral beam etching is smaller than that of reactive ion etching. However, a low directional ratio below 30% can produce a large change in the etching rate. Therefore, a high directional ratio of the neutral angle of more than 50% is required for high-performance neutral beam etching.

5. Conclusions

In neutral beam etching, systematic parameters, such as pressure and reflector length, are required to be set for anisotropic etching. The neutral angle distribution is dependent on reflector length because of the blocking of high-angle neutrals. Background gases in the chamber cause sidewall etching. The effect of background gases is diminished for anisotropic etching. The neutral flux from the neutral beam source should be much larger than that from background gases. As pressure decreases, the neutral fluxes from both background gases and the neutral beam source also decrease. To verify this, we simulated a low-angle-reflector neutral beam source. The neutral flux from this source was much larger than that from background gases at gas pressures less than 0.5 mTorr. Therefore, a low gas pressure of less than 0.5 mTorr leads to vertical etching.

Generally, reactive ion etching causes charge-up damage such as RIE lag and the microloading effect. RIE lag is explained by surface charge and radical transport. In our charging simulations, a change in ion flux as a function of

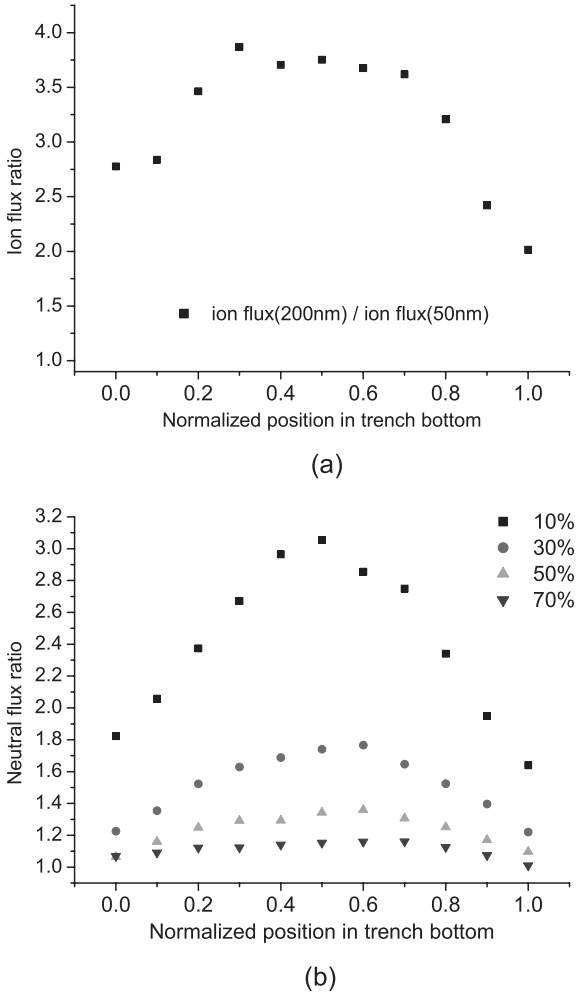

Fig. 10. (a) Ion flux ratio of reactive ion etching and (b) neutral flux ratio of neutral beam etching for comparison of 200 nm and 50 nm trenches.

trench width was observed. The surface charge-up potential creates a large gradient of the ion flux ratio. The ion flux in the 200 nm trench was approximately four times larger than that in the 50 nm trench. This gradient of the ion flux ratio as well as the radical transport results in RIE lag and the microloading effect.

In neutral beam etching, surface charging effects are eliminated due to the use of uncharged particles. The neutral beam source, which controls radicals directly, removes the RIE lag and the microloading effect caused by the radical transport and surface charges. The neutral angle distribution is an important factor for reducing the gradient of the etching rate. The neutral flux in the 200 nm trench is approximately two times larger than that in the 50 nm trench for the directional ratio of 30%. The low directional ratios of neutral angles of less than 50% result in sidewall etching and large gradients of etching rate like RIE lag. It causes bowing for a trench size ranging from 50 to 200 nm. Therefore, for the pressure and neutral beam angle, a neutral beam source requires a pressure of less than 0.5 mTorr and a directional ratio of neutral angles of more than 50% to achieve high-performance neutral beam etching.

Acknowledgements

The authors would like to thank Dr. N. Babaeva, and Mr. H. S. Park for their advice and discussions. This work was supported in part by Tera-level Nano Devices Project, 21*c* Frontier R&D Program, Korea Ministry of Science and Technology.

1) F. F. Chen: Phys. Plasmas **2** (1995) 2164.
2) M. A. Lieberman and A. J. Lichtenberg: *Principles of Plasma Discharges and Materials Processing* (John Wiley & Sons, New York, 1994).
3) R. A. Gottscho, C. W. Jurgensen and D. J. Vitkavage: J. Vac. Sci. & Technol. B **10** (1992) 2133.
4) K. Hashimoto: Jpn. J. Appl. Phys. **33** (1994) 6013.
5) T. Kinoshita, M. Hane and J. P. Mcvittie: J. Vac. Sci. & Technol. B **14** (1996) 560.
6) J. Matsui, N. Nakano, Z. L. Petrovic and T. Makabe: Appl. Phys. Lett. **78** (2001) 883.
7) G. S. Hwang and K. P. Giapis: Appl. Phys. Lett. **74** (1999) 932.
8) K. P. Giapis, T. A. Moore and T. K. Minton: J. Vac. Sci. & Technol. A **13** (1995) 959.
9) S. Samukawa, K. Sakamoto and K. Ichiki: Jpn. J. Appl. Phys. **40** (2001) L997.
10) K. Yokogawa, T. Yunogami and T. Mizutani: Jpn. J. Appl. Phys. **35** (1996) 1901.
11) S. R. Leone: Jpn. J. Appl. Phys. **34** (1995) 2073.
12) M. J. Gechner, T. K. Bennett and S. A. Cohen: Appl. Phys. Lett. **71** (1997) 980.
13) M. S. Hur, S. J. Kim, H. S. Lee, J. K. Lee and G. Y. Yeom: IEEE Trans. Plasma Sci. **30** (2002) 110.
14) J. P. Verboncoeur, A. B. Langdon and N. T. Gladd: Comput. Phys. Commun. **87** (1995) 199.
15) D. H. Lee, M. J. Chung, S. D. Park and G. Y. Yeom: Jpn. J. Appl. Phys. **41** (2002) L1412.
16) J. F. Ziegler, J. P. Biersack and U. Littmark: *The Stopping and Range of Ions in Solids* (Pergamon, New York, 1985).
17) W. Eckstein and J. P. Biersack: Appl. Phys. A **38** (1985) 123.
18) Y. Tokunaga, Y. Kurita, M. Sugihara, S. Hitoki and S. Saito: Comput. Phys. Commun. **38** (1985) 15.
19) C. A. Nichols and D. M. Manos: J. Appl. Phys. **80** (1996) 264.
20) B. A. Helmer and D. B. Graves: J. Vac. Sci. & Technol. A **16** (1998) 3502.
21) C. F. Abrams and D. B. Graves: J. Vac. Sci. & Technol. A **16** (1998) 3006.
22) J. I. Ulacia and J. P. McVittie: J. Appl. Phys. **65** (1989) 1484.
23) K. Ninomiya, K. Suzuki, S. Nishimatsu and O. Okada: J. Appl. Phys. **58** (1985) 1177.
24) S. J. Kim, S. J. Wang, J. K. Lee, D. H. Lee and G. Y. Yeom: to be published in J. Vac. Sci. & Technol. A **22** (2004).
25) H. S. Park, S. J. Kim, Y. Q. Wu and J. K. Lee: IEEE Trans. Plasma Sci. **31** (2003) 703.